Accepted Manuscript

Title: Droplet Deformation under Pulsatile Electric Fields

Authors: Bin Li, Vincenzino Vivacqua, Mojtaba Ghadiri,
Zhiqian Sun, Zhenbo Wang, Xiaoyu Li

Please cite this article as: Li, Bin, Vivacqua, Vincenzino, Ghadiri, Mojtaba, Sun, Zhiqian, Wang, Zhenbo, Li, Xiaoyu, Droplet Deformation under Pulsatile Electric Fields.Chemical Engineering Research and Design https://doi.org/10.1016/j.cherd.2017.09.024

Droplet Deformation under Pulsatile Electric Fields

Bin Li[a,b], Vincenzino Vivacqua[b], Mojtaba Ghadiri[b, *1], Zhiqian Sun[a], Zhenbo Wang[a],

Xiaoyu Li[a]

[a] State Key Laboratory of Heavy Oil, China University of Petroleum (East China), Qingdao 266580, Shandong, China

[b] Institute of Particle Science and Engineering, University of Leeds, School of Chemical and Process Engineering, Leeds LS2 9JT, UK

[*] Corresponding author. Fax: +44 113 343 2384.

E-mail address: M.Ghadiri@leeds.ac.uk (M. Ghadiri).

Graphical abstract
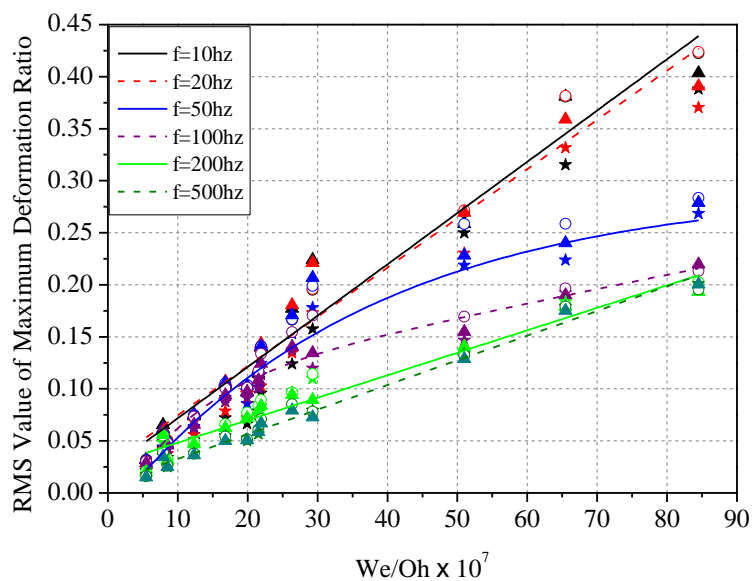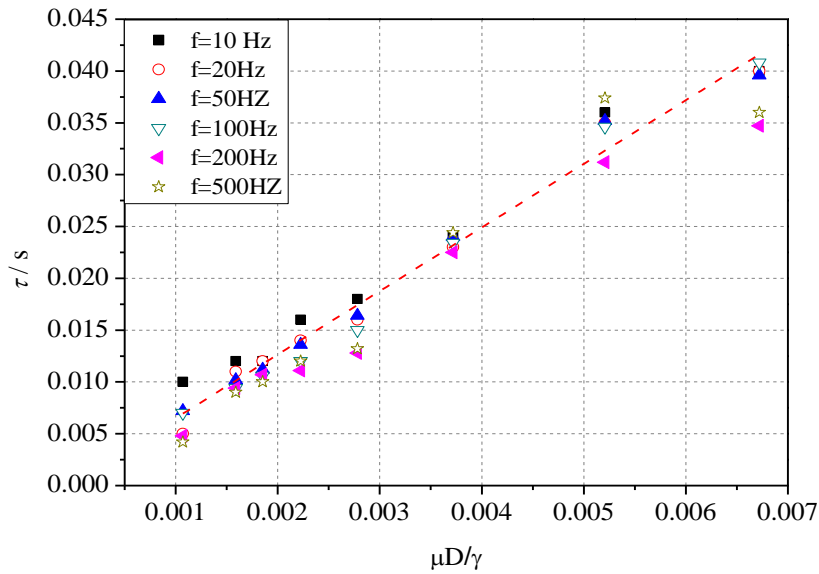
Highlights

- Drop deformation dynamics under pulsatile electric fields is analysed.

- A good quantitative agreement with experimental data is obtained.

- The effects of electrical and physical parameters are quantified.

- Results are compared with a linear model of the same process.

- The ratio of Weber number and Ohnesorge number describes droplet deformation well.

Abstract: The deformation of a water droplet in a dielectric oil phase in the presence of externally pulsatile electric fields is numerically analysed with the finite element method. The proprietary software Comsol Multiphysics is used to conduct the simulation and the motion of the interface is captured by the Level-Set method. Experimental work is conducted to validate the model, and found to be in good agreement with the numerical results. The effects of electric field type, electric field

intensity, electric field frequency, droplet size, surface tension, and bulk phase viscosity have been systematically assessed. The electric field strength induces droplet deformation, opposed by surface tension and viscosity. The ratio of Weber Number (describing electric field effects) and Ohnesorge Number (describing physical properties) is found to describe the droplet deformation well for the low frequency range, where the time for the droplet to reach stationary shape is shorter than the electric field half-period. Here a linear relationship is found to prevail between the RMS value of deformation ratios DR as a function of We/Oh. At higher frequencies, where the electric field half period becomes much shorter than the mechanical response time the functional dependence becomes first non-linear and then eventually approaches that of the constant electric field at equivalent RMS strength. The outcome of this work is potentially useful for optimizing the design of oil-water separation devices.

Keywords: Droplet deformation; Pulsatile electric fields; Level-Set method; Interface; Electrohydrodynamics

1. Introduction

Water-in-oil emulsions are readily formed during the production of crude oil and cause detrimental problems at several stages of production [1]. The slow rate at which the dispersed phase naturally settles down from such emulsions has a significant influence on the oil industry [1, 2]. Moreover, crude oil contains resins, asphaltenes, and paraffins, which stabilize the emulsion as they act as surfactant, causing a much more difficult oil-water separation [3]. Therefore, methods that allow efficient

removal of a dispersed water phase from a continuous oil phase are highly desirable and will have remarkable economic benefits for the oil industry. Several techniques [4-8] are utilized to enhance the separation of water-in-oil emulsions. Electrostatic demulsification is one of the most effective and widely utilised methods [3,9]. The state of understanding of the electrocoalescence has recently been reviewed by Mhatre et al. [10]. An externally applied electric field can accelerate drainage of the oil film between two coalescing water droplets to promote the process of coalescence and separation of water from oil [10, 11]. However, Mousavi et al. [12-14] reported that partial coalescence could occur when the electric field intensity was excessively high or droplets were large. Moreover, excessively high electric field intensity results in the formation of Taylor cones, causing electro-spraying, which has adverse effects on the separation efficiency of water droplets from the oil.

Droplet deformation in the presence of an externally applied electric field is very common in many industries, including electrospining [15], electrospraying [16] and electrowetting [17], etc. A good number of experimental and numerical works have been conducted on droplet deformation under an electric field [18-24]. Taylor [25] proposed an electrohydrodynamic model, generally referred as the "leaky dielectric model", for droplet deformation, with the assumptions of neutral droplets, quasi-static electric field, small deformation, and free convection charge. The model fitted well with the experimental results at small deformations, while deviations occurred when the droplet deformed extensively [26]. Recently, Teigen et al. [27] also adopted the "leaky dielectric model" to investigate the influence of surfactant on drop deformation,

which shows that the presence of surfactant can either increase or reduce the deformation, depending on the shape of the deformation and the direction of the electrically induced circulation. Moreover, a number of new models have been proposed over the past decades [26, 28, 29]. Most recently, Vivacqua et al. [18] proposed a linear dynamics model under pulsatile fields with various waveforms as forcing terms, namely half-sinusoidal, square and sawtooth waves. They reported that the droplet deformation was affected by the electric field type stimulus. Moreover, their results illustrated that the droplet deformation follows a pattern of driven damped harmonic oscillator, with the damping ratio and dimensionless eigen frequency depending on Ohnesorge number and Weber number, respectively.

Numerical simulations of droplet behaviour have been carried out to describe the droplet interface explicitly and implicitly by using interface tracking and interface capturing methods, respectively. In the former, discrete points are tracked on the interface surface, including front tracking method and boundary integral method [30]. However, these methods are not straightforward because surface-marker points are usually needed to track the droplet behaviour, such as deformation and coalescence. On the other hand, the implicit methods, Level-Set, Volume of Fluid (VOF) and Phase-Field, are better suited to the calculation of large topological deformations [31]. The interface is modelled by an additional transport equation and treated as a material line propagating with the fluid [31]. Vivacqua et al. [32] investigated the coalescence of a water drop in a dieletric oil phase at the oil-water interface under a constant electric field by the Level-Set method. They reported the effects of some input

5

parameters, including the mesh size, interface thickness, re-initialization parameter, droplet size and water conductivity, on the model prediction. Their simulation work showed a good agreement with the experimental work conducted by Mousavichoubeh et al. [14], predicting that the partial droplet coalescence is mainly regulated by a combination of the electrical Weber number and Ohnesorge number. He et al. [23] investigated the transient response of droplet deformation in a constant electric field by the Level-Set method as well, showing good agreement with the experimental work. Bjørklund [33] studied droplet breakup and drop-drop coalescence due to the electrically induced forces by a combination of the Level-Set method and the Ghost-Fluid method. His work showed that the Level-Set method is capable of modelling the droplet dynamics before, during, and after coalescence of droplets. Lopez-Herrera et al. [34] conducted numerical simulations on two-phase electrohydrodynamic problems by VOF method. Their simulation work accurately predicted the time evolution of charge distribution and droplet deformation. A number of simulation studies [35-39] have been conducted on droplet deformation. However, most of the investigations are focused on steady electric field, and very few papers address the effect of pulsatile electric fields on the deformation process. The aim of this work is to provide a mathematical description of droplet deformation under pulsatile electric fields in the case of half-sinusoidal, square and sawtooth waves. For this purpose, a finite element approach combined with the Level-Set method [39] is adopted to analyse the process of droplet deformation. The present study reports the effects of key factors, including externally applied electric field type, electric field

intensity, electric field frequency, droplet size, surface tension and bulk phase viscosity.

2. Model description

The computational model uses a 2-D axisymmetric domain and schematically shown in Fig. 1(a). A close-up of the domain near the oil-water interface is shown in Fig. 1(b) to show the quality of the mesh generated with $h_{max}/D=0.03$, where h_{max} is the maximum mesh element size and D is droplet diameter. The boundary conditions used in this paper are as follows: the upper boundary is with a pulsatile electric potential (U(t)), while the opposite one is kept earthed and both boundaries have no-slip conditions; the right boundary is a slip one ($\mathbf{u} \cdot \mathbf{n}=0$), as this allows significant reduction of the simulation domain. The Bond number $B_o = \Delta\rho g r^2/\gamma \ll 1$, where r is droplet radius, which means that the body force is much smaller compared to surface tension force. Therefore, the gravitational effects are neglected in this paper. Moreover, the droplet is considered as a conductor so that the electric field inside it can be ignored; the electrokinetic effects are also neglected as the droplet net charge is zero.

The Level-Set method is employed to track the boundaries between continuous oil phase and dispersed water phase. The location of interface is obtained by solving the transport equation of the Level-Set function ϕ, described by $\phi=0.5$ [23, 32]. The evolution of the boundary is given by Eq. (1), first proposed by Olsson and Kreiss [40].

$$\frac{\partial \phi}{\partial t} + \mathbf{u}\nabla\phi = \lambda\nabla \cdot (\xi\nabla\phi - \phi(1-\phi)\frac{\nabla\phi}{|\nabla\phi|}) \qquad (1)$$

7

where $\mathbf{u}$ is fluid velocity, ϕ is a smooth step function which varies from 0 to 1, λ is a re-initialization parameter, which gives stability to the solution and ξ is related to the interface thickness.

The interface is modeled as a diffuse boundary. A preliminary step computes the distance between the initial interface and the nodes of the computational domain, D_{si}. The initial condition for the time dependent study is then calculated as:

$$\phi = \frac{1}{1+e^{\pm D_{si}/\xi}} \qquad (2)$$

The positive sign is used in Eq. (2) for points initially inside the interface, whereas the minus sign applies to the domain outside the interface. The interface is described by the Level-Set $\phi = 0.5$. The variable increases to 1 and decreases to 0 exponentially outside and inside the droplet, respectively.

We follow the approach of Vivacqua et al. [32], coupling Eq. (1) with the Navier Stokes equations for the flow and Laplace equations for the electric field. The capillary and electrostatic forces are also included in the Navier Stokes equations shown as follows.

$$\rho(\phi)\frac{\partial \mathbf{u}}{\partial t} + \rho(\phi)(\mathbf{u}\cdot\nabla)\mathbf{u} = -\nabla p + (\mu(\phi)(\nabla\mathbf{u} + \nabla\mathbf{u}^{\mathrm{T}})) + \mathbf{F}_{\gamma} + \mathbf{F}_{\mathbf{E}} \qquad (3)$$

$$\nabla \cdot \mathbf{u} = 0 \qquad (4)$$

$$\rho(\phi) = \rho_{w} + (\rho_{o} - \rho_{w})\phi \qquad (5)$$

$$\mu(\phi) = \mu_{w} + (\mu_{o} - \mu_{w})\phi \qquad (6)$$

where p is the fluid pressure, $\mathbf{F}_{\gamma}$ is the interfacial force of oil and water phase, $\mathbf{F}_{\mathbf{E}}$ is the electric force, ρ_{w} is water phase density, ρ_{o} is oil phase density, μ_{w} is water phase viscosity and μ_{o} is oil phase viscosity.

The interfacial force ($\mathbf{F}_\gamma$) is calculated as derived by:

$$\mathbf{F}_\gamma = \nabla \cdot (\gamma (\mathbf{I} - (\mathbf{nn}^{\mathrm{T}}))\delta) \tag{7}$$

where γ is the surface tension coefficient, $\mathbf{I}$ is the identity matrix, $\mathbf{n}$ is the interface normal, and δ is a smooth approximation of the Dirac function. $\mathbf{n}$ and δ are obtained by calculating Eq. (8) and (9), respectively:

$$\mathbf{n} = \frac{\nabla \phi}{|\nabla \phi|} \tag{8}$$

$$\delta = 6 |\nabla \phi| |\phi (1 - \phi)| \tag{9}$$

The electric force is obtained from the divergence of the Maxwell stress tensor:

$$\mathbf{F}_{\mathbf{E}} = \nabla \cdot (\varepsilon(\phi)\mathbf{E}\mathbf{E}^{\mathrm{T}} - \frac{1}{2}\varepsilon(\phi)(\mathbf{E} \cdot \mathbf{E})\mathbf{I}) \tag{10}$$

$$\varepsilon(\phi) = \varepsilon_{\mathrm{w}} + (\varepsilon_{\mathrm{o}} - \varepsilon_{\mathrm{w}})\phi \tag{11}$$

where $\mathbf{E}$ is the electric field intensity, ε_{w} is water phase permittivity, ε_{o} is oil phase permittivity. $\mathbf{E}$ can be determined by solving the charge conservation equation:

$$\nabla(\sigma(\phi)\mathbf{E} + \varepsilon(\phi)\frac{\partial \mathbf{E}}{\partial \mathrm{t}}) = 0 \tag{12}$$

$$\sigma(\phi) = \sigma_{\mathrm{w}} + (\sigma_{\mathrm{o}} - \sigma_{\mathrm{w}})\phi \tag{13}$$

where σ_{w} is water phase conductivity, σ_{o} is oil phase conductivity.

In this approach, the Level-Set function is initialized as a distance function [41] as is shown in Eq. (2). Numerical errors result in fluctuating distance function when the Level-Set function moves with the fluid, accounting for changing interface thickness. Procedures for re-initialization are therefore needed to keep the thickness constant. The parameter λ in Eq. (1) influences the numerical stabilization significantly. λ should be optimized for a specific case, because, too small λ leads to

non-preserved interface thickness, while too large λ results in incorrect interface movement and convergence problems. For our case, we have analysed the sensitivity of model predictions to λ for the range λ=0.01 m/s, 0.1 m/s, 1.0 m/s (not shown here), where the simulation run successfully. However, we find that λ does not bring about appreciable changes on the calculation of deformation and hence we adopt λ=1 m/s for the rest of the calculations.

The interface thickness is determined by the parameter ξ through Eq. (2). ξ describes the rapidity by which the Level-Set function varies with the distance of the domain points from the 0.5 Level-Set iso-contour. The sensitivity of the result to ξ is also tested in the range ξ/D=0.018-0.022. Outside this range convergence problems were experienced, so ξ/D=0.020 was used for all calculation.

3. Experimental set-up

The experimental cell [14,42] is made of Perspex to facilitate visualization of deformation process (Fig. 2). The electrodes are polished brass plates with dimensions of 90 mm $\times$ 25 mm. The upper electrode is set at 30 $\pm$ 0.5 mm from the grounded electrode. The high voltage electrode is connected to a waveform generator, feeding a Trek 20/20C high voltage amplifier. The bottom electrode is grounded. A high-speed digital video camera (Photron FASTCAM SA5), equipped with a micro-lens (NAVITAR 12 $\times$ Zoom Lens) is used to observe the deformation phenomenon. The camera is used with a frame speed of 20,000 frames per second. The physical properties of the sunflower oil/water emulsion, as measured by Mousavichoubeh et al. [14], are shown in Table 1. For electrocoalescence the dispersed aqueous phase should

have electrical conductivity and permittivity significantly higher than those of the continuous phase (dielectric oil). According to the parameters shown in Table 1, the system of interest (i.e. deionised water droplets in sunflower oil) satisfies the above criterion. Water droplets are introduced into the cell through a hole in the centre of the high voltage electrode by a Hamilton micro-litre syringe.

The droplet deformation ratio, DR, is defined by Eq. (13):

$$DR = \frac{A - B}{A + B} \qquad\qquad (14)$$

where A and B are the axis lengths of the elliptic droplet which are parallel and perpendicular to the direction of the externally applied electric field, respectively. A positive DR represents a deformation to a prolate shape (parallel to the electric field direction), while a negative DR to oblate shape (perpendicular to electric field direction) (Fig. 3).

4. Results

4.1 Experimental validation

The experimental and numerical conditions are as follows: electric field strength: $E = 533$ V mm^{-1}; droplet diameter: $D = 1.196$ mm and 2.8 mm, respectively; electric field type: half-sinusoidal, square and sawtooth waves, respectively; the interfacial tension between deionized water and sunflower oil is $\gamma = 0.025$ N m^{-1}, as given by Mousavi et al [13]. The relative difference between experimental measurements and simulation results is given by $\frac{\Delta DR}{DR} = \frac{2||DR_e| - |DR_s||}{|DR_e| + |DR_s|}$ following the approach of Berg et al. [43], where DR$_e$ is experimental deformation ratio and DR$_s$ is numerical deformation ratio. The experimental and simulated deformation ratios are compared in

Fig. 4 for the sawtooth electric field type, where a good agreement is observed, having a relative difference of less than 13 %. The other two electric field types produce a similar agreement. The grid dependence has been checked by carrying out a sensitivity analysis of the deformation ratio for the following number of grids: 16252, 19128 and 24100. Considering both the accuracy and the computational time, 19128 grids were adopted in our simulation work. The time step length used in the simulation are: 0.02s for 1 Hz; 0.002s for 10 Hz; 0.001s for 20 Hz; 0.0004s for 50 Hz; 0.0002s for 100 Hz; 0.0001s for 200 Hz; 0.00004s for 500 Hz.

4.2 Effect of electric field frequency

We define a dimensionless time as:

$$T=tf \tag{15}$$

where f is the frequency of the applied electric field. The deformation ratio is shown as a function of tf (T) for the three wave forms at 10, 50 and 500 Hz in Fig. 5. At low frequencies (f ≤10 Hz), the droplet deformation follows the forcing function as the time to reach stationary shape is short as compared to the electric field half period. The droplet with half-sinusoidal wave has the minimum negative deformation (oblate form), while square and sawtooth waves have similar deformation extent in this region. The reason for the difference in the extent of deformation between the three wave forms might be that the electric stress vanishes very fast for square and sawtooth waves. The interface acceleration, resulting from surface tension, is larger than that of half-sinusoidal waves, accounting for larger interface velocity.

At 50 Hz, the deformation phase is delayed. In the case of the square wave, in

12

the region where the electric field is steady, the deformation is not stable. At 500 Hz, the droplet deformation loses the electrical forcing pattern completely. It increases gradually first and then decreases to a quasi-steady state with slight fluctuations. This is because, increasing the frequency, a point is reached where the period of the electric field becomes shorter than the mechanical relaxation time and hence the frequency of droplet oscillation can no longer follow the field frequency [12]. At a high frequency (f $\geq$500 Hz), the deformation process is similar to the pattern of constant electric field [44]. Lesaint et al. [45] reported that the root mean square (RMS) of the electric field can represent the effectiveness of different electric field waveforms. The theoretical RMS values of the electric field of the three waveforms used here are shown in Table 2, according to which, droplets under half-sinusoidal and square waves should have similar deformations, whereas the sawtooth wave should produce smaller deformations. A similar pattern prevails in Fig. 5, particularly notable at 500 Hz. Moreover, the deformation values should be the same as that of the constant field if RMS values of different waveforms are considered. This is quantitatively verified and shown in Fig. 6. Here the RMS values of the deformation ratio, taken as the deformation ratio multiplied by the relevant RMS factor, are plotted as a function of time for the constant, half-sinusoidal, square and sawtooth waveform electric fields. On the application of the electric field an overshoot occurs in the droplet deformation, but for all the three wave forms a constant asymptotic value of deformation ratio is obtained which is nearly coincident with the constant electric field.

5. Discussion

The trends of literature data can now be compared with the simulation work presented here. For this purpose, a new dimensionless deformation ratio and oscillation amplitude are defined as $DR' = \frac{A-D}{A_{ss}-D}$ and $A'_m = \frac{DR'_{max}}{DR'_{min}}$, where A_{ss} is the steady state droplet diameter along externally applied constant electric field, and D is initial droplet diameter. In Fig. 7, the linear model predictions of Vivacqua et al. [18] are compared with the simulation results for identical conditions in terms of amplitude of the oscillatory response. The results of simulation and linear model have similar trends, especially at high frequencies (f ≥ 100Hz). However, at low frequencies (10-50 Hz), the difference is significant. This is probably caused by the small deformations approximation that the linear model adopted. Nevertheless, a qualitative agreement between the two approaches prevails. From Fig. 7, it is concluded that with pulsatile fields, the oscillation amplitude can have a maximum value at an intermediate frequency if the Ohnesorge number, $\text{Oh} = \dfrac{\mu}{\sqrt{\rho \gamma \text{D}}}$, is lower than one. As the Ohnesorge number is decreased to very low values in the case here around 0.0578, the oscillation amplitude becomes very large. This is undesirable as it would lead to droplet disintegration. Fig. 7 also shows that the oscillation amplitudes are negligible at high frequencies (f > 500 Hz). Low oscillation amplitudes are likely to suppress the occurrence of secondary droplets [18]. In addition, it is seen in Fig. 5 that high frequencies have lower deformation ratio. Therefore, at high frequencies, droplets are more stable, accounting for decreasing volume fraction of secondary droplets formed due to partial coalescence experimentally obtained by Mousavichoubeh et al. [12]. Stronger electric fields can therefore be applied to the water-in-oil emulsions at high

frequencies. However, some oscillatory behaviour can be beneficial in weakening the stability of the interfacial film during drop-drop coalescence, as it is also claimed in commercial electrocoalescers [10]. These devices, however, operate in the kHz range of frequency, where no oscillation probably occurs.

The current state of understanding [14,18,20] points to two dimensionless groups, the electrical Weber Number, $We = \dfrac{\varepsilon_0 \varepsilon_{oil} E^2 D}{\gamma}$, accounting for the extent of deformation under an electric field, and Ohnesorge Number accounting for the rate of deformation. The deforming process is a competing process between the electrostatic stress and interfacial tension, and its deformation rate is affected by the bulk viscosity. Therefore, the coupling effects of We and Oh on DR can be described with the following combination of these two dimensionless numbers:

$$We/Oh = \frac{\rho^{0.5} \varepsilon_0 \varepsilon_{oil} E^2 D^{1.5}}{\mu \gamma^{0.5}} \qquad (4)$$

The RMS value of the maximum deformation ratio DR as a function of We/Oh is shown in Fig. 8, where a linear trend is observed at low frequencies (10 and 20 Hz) with data overlapping for all the waveforms. However, at frequencies of 50 and 100 Hz, the variation of the deformation ratio versus We/Oh becomes non-linear. At 200 Hz and above the deformation varies again linearly with We/Oh. These results can be interpreted in the light of the time (τ) required for the droplet to reach its stationary shape, having gone through the oblate shape form transformation. This is obtained by applying a single step change in the electric field and calculating the time interval necessary for the droplet to reach a zero deformation value after the first stage of passing through an oblate shape, as shown in Fig. 9. For a range of bulk viscosities

(46.5-120.0 mPa s), surface tensions (0.016-0.035 N/m) and droplet sizes (0.576-2.800 mm) as given in Table 3, time to reach stationary shape (τ) follows a functional relationship with the dimensionless group $\mu D/\gamma$, as shown in Fig. 10. This implies that at low viscosities, the droplet can respond to high frequencies, i.e. deforming and assuming a shape as shown in Fig. 5 (a) & (b) for which τ is shorter than the electric field half period. In contrast, at high viscosities, τ increases and the droplet can no longer respond to a high frequency variations of the electric field as shown in Fig. 5 (c). The ratio of electric half period and τ is shown in Table 4, which shows that, at low frequencies (f≤20 Hz), the electric field period is longer than or close to τ at the investigated We/Oh numbers, so that the process is independent of the electric field frequency. At 50 Hz, the ratio of electric field period and τ is close to 1 at low We/Oh numbers, while it decreases remarkably at high We/Oh numbers, resulting in a reduction of deformation. At high frequencies (f≥200Hz), the electric period is much shorter than τ for all We/Oh numbers, and the deformation becomes again insensitive to the applied electric frequency. It is noteworthy that whilst the ratio We/Oh describes well the deformation behaviour, the mechanism of secondary droplet formation is, in contrast, better described by the product of the Weber number and Ohnesorge number, as shown previously by Mousavichoubeh [14]. This suggests that once the droplet is ruptured, other electromechanical mechanisms become operative. Further work is needed to analyse the secondary droplet formation by the above approach to elucidate the exact role of various mechanisms in secondary droplet formation.

16

6. Conclusions

Droplet deformation in the presence of externally pulsatile electric fields, namely, half-sinusoidal wave, square wave and sawtooth wave, has been analysed with Level-Set Method describing the interface. The effects of electric field type, electric field intensity, electric field frequency, droplet size, surface tension, and oil phase viscosity have been assessed. Deformation ratio is introduced to represent the extent of oscillation. Experimental work is conducted to validate the model. Good agreement is obtained between numerical and experimental results, indicating that the model is capable of reproducing droplet deformation under pulsatile electric fields. The qualitative agreement between the previous linear model predictions and the simulation results and their quantitative differences clearly identifies the operative range of the former.

The deforming process is a competing process between the electrostatic stress and interfacial tension, determined by the coupling effects of Weber Number and Ohnesorge Number. The ratio We/Oh is found to describe the deformation process, showing a good unification of data at low frequencies. It has also been shown that the oscillation amplitude can become unbounded at low values of the Ohnesorge number. This should be avoided as it can have detrimental effects on the separation efficiency in electrocoalescers. This study can potentially be useful in the selection of the optimum electric field conditions to maximize the efficiency of electrocoalescers and optimise the design of oil-water separation devices.

References

[1] C. Tsouris, W.T. Shin, S. Yiacoumi, Pumping, spraying, and mixing of fluids by electric fields, Can. J. Chem. Eng, 76 (3) (1998) 589-599.

[2] S.E. Taylor, Theory and practice of electrically-enhanced phase separation of water-in-oil emulsion, Trans. IChemE, 74 (5) (1996) 526-540.

[3] B. Li, Z. Sun, Z. Wang, Y. Jin, Y. Fan, Effects of high-frequency and high-voltage pulsed electric field parameters on water chain formation, J. Electrostat. 80 (2016) 22-29.

[4] R.A. Mohammed, A.I. Baile, P.F. Luckham, S.E. Taylor, Dewatering of crude oil emulsions 3, Colloids Surf. A, 83 (3) (1994) 261-271.

[5] D. Sun, S.C. Jong, X.D. Duan, D. Zhou, Demulsification of water-in-oil emulsion by wetting coalescence materials in stirred- and- packed columns, Colloids Surf. A., 150 (1-3) (1999) 69-75.

[6] M. Goto, J. Irie, K. Kondo, F. Nakashio, Electrical demulsification of w/o emulsion by continuous tubular coalesce, J. Chem. Eng. Jpn., 22 (4) (1989) 401-406.

[7] R.A. Mohammed, A.I. Baile, P.F. Luckham, S.E. Taylor, Dewatering of crude oil emulsions 4, Colloids and Surfaces A, 80 (2&3) (1993) 223-235.

[8] T. Hirato, K. Koyama, T. Tanaka, Demulsification of water-in-oil emulsion by an electrostatic coalescence method, Mater Trans.32 (3) (1991) 257-263.

[9] J.S Eow, M. Ghadiri, Electrostatic enhancement of coalescence of water droplets in oil: a review of the technology, Chem. Eng. J. 85 (2-3) 357-368.

[10] S. Mhatre, V. Vivacqua, M. Ghadiri, A.M. Abdullah, M.J. AI-Marri, A. Hassanpour, B. Hewakandamby, B. Azzopardi, B. Kermani, Electrostatic phase separation: A review, Chem. Eng. Res. Des., 96 (2015) 177-195.

[11] V. Vivacqua, S. Mhatre, M. Ghadiri, A.M. Abdullah, A. Hassanpour, M.J. AI-Marri, B. Azzopardi, B. Hewakandamby, B. Kermani, Electrocoalescence of water drop trains in oil under constant and pulsatile electric fields, Chem. Eng. Res. Des., 104 (2015) 658-668.

[12] S.H. Mousavi, M. Ghadiri, M. Buckley, Electro-coalescence of water drops in oils under pulsatile electric fields, Chem. Eng. Sci., 120 (2014) 130-142.

[13] M. Mousavichoubeh, M. Ghadiri, M. Shariaty-Niassar, Electro-coalescence of an aqueous droplet at an oil–water interface, Chem. Eng. Process. 50 (3) (2011) 338-344.

[14] M. Mousavichoubeh, M. Shariaty-Niassar, M. Ghadiri, The effect of interfacial tension on secondary drop formation in electro-coalescence of water droplets in oil, Chem. Eng. Sci., 66 (21) (2011) 5330-5337.

[15] H. Yoshimoto, Y.M. Shin, H. Terai, J.P. Vacanti, A biodegradable nanofiber scaffold by electrospinning and its potential for bone tissue engineering, Biomaterials 24 (2003) 2077-2082.

[16] A. Ganan-Calvo, Erratum: cone-jet analytical extension of Taylor's electrostatic solution and the asymptotic universal scaling laws in electrospraying, Phys. Rev. Lett. 85 (2000) 4193.

[17] S.K. Cho, H. Moon, C.J. Kim, Creating, transporting, cutting, and merging liquid

droplets by electrowetting-based actuation for digital microfluidic circuits, J. Microelectromech. Syst. 12 (2003) 70-80.

[18] V. Vivacqua, M. Ghadiri, A.M. Abdullah, A. Hassanpour, M.J. AI-Marri, B. Azzopardi, B. Hewakandamby, B. Kermani, Linear dynamics modeling of droplet deformation in a pulsatile electric field, Chem. Eng. Res. Des., 114 (2016) 162-170.

[19] H. Yan, L. He, X. Luo, J. Wang, X. Huang, Y. Lü, et al., Investigation on transient oscillation of droplet deformation before conical breakup under alternating current electric field, Langmuir 31 (2015) 8275-8283.

[20] J.S. Eow, M. Ghadiri, Motion, deformation and break-up of aqueous drops in oils under high electric field strengths, Chem. Eng. Process 42 (2003) 259-272.

[21] O. Vizika, D.A. Saville, The electrohydrodynamic deformation of drops suspended in liquids in steady and oscillatory electric fields, J. Fluid Mech. 239 (1992) 1-21.

[22] D.A. Saville, ELECTROHYDRODYNAMICS: the taylor-melcher leaky dielectric model, Annu. Rev. Fluid Mech. 29 (1997) 27-64.

[23] L. He, X. Huang, X. Luo, H. Yan, Y. Lu, D. Yang, Y. Han, Numerical study on transient response of droplet deformation in a steady electric field, J. Electrostat. 82 (2016) 29-37.

[24] J. Raisin, J.-L. Rebound, Electrically induced deformations of water-air and water-oil interfaces in relation with electrocoalescence, J. Electrostat. 69(2011)275-283.

[25] G. Taylor, Studies in electrohydrodynamics, I. Circulation produced in a drop by electric field, Proc. R. Soc. A. 291 (1966) 159-166.

[26] S. Torza, R.G. Cox, S.G. Mason, Electrohydrodynamic deformation and burst of liquid drops, Philos. Trans. R. Soc. A. 269 (1971) 295-319.

[27] K.E. Teigen, S.T. Munkejord, Influence of surfactant on drop deformation in an electric field, PHYS. FLUIDS. 112104 (2010) 1-10.

[28] K. Emilij, An electrokinetic model of drop deformation in an electric field, J. Fluid Mech. 472 (2002) 1-27.

[29] B. Nikolaos, K. Sonja, Droplet deformation in dc electric fields: the extended leaky dielectric model, Langmuir, 21 (2005) 6194-6209.

[30] R.T. Collins, J.J. Jones, M.T. Harris, O.A. Basaran, Electrohydrodynamic tip streaming and emission of charged drops from liquid cones, Nat. Phys. 2 (2008)149-154.

[31] M.S. Shadllo, A. Rahmat, M. Yildiz, A smoothed particle hydrodynamics study on the electrohydrodynamic deformation of a droplet suspended in a neutrally buoyant Newtonian fluid, Comput. Mech. 52 (2013) 693-707.

[32] V. Vivacqua, M. Ghadiri, A.M. Abdullah, A. Hassanpour, M.J. AI-Marri, B. Azzopardi, B. Hewakandamby, B. Kermani, Analysis of partial electrocoalescence by Level-Set and finite element methods, Chem. Eng. Res. Des. 114(2016)180-189.

[33] E. Bjørklund, The level-set method applied to droplet dynamics in the presence of an electric field, COMPUT. FLUIDS. 38 (2009) 358-369.

[34] J.M. Lopez-Herrera, S. Popinet, M.A. Herrada, A charge-conservative approach for simulating electrohydrodynamic two-phase flows using volume-of-fluid, J. Comput. Phys. 230 (2011) 1939-1955.

[35] J.Q. Feng, T.C. Scott, A computational analysis of electrohydrodynamics of a leaky dielectric drop in an electric field, J. Fluid Mech. 311 (1996) 289-326.

[36] E. Lac, G.M. Homsy, Axisymmetric deformation and stability of a viscous drop in a steady electric field, J. Fluid Mech. 590 (2007) 239-264.

[37] Y. Yao, Y. Wang, K.M. Beussman, Deformation and migration of a leakydielectric droplet in a steady non-uniform electric field, Microfluid. Nanofluid 17 (2014) 907-921.

[38] J.W. Ha, S.M. Yang, Deformation and breakup of Newtonian and non-Newtonian conducting drops in an electric field, J. Fluid Mech. 405 (2000) 131-156.

[39] J.A. Sethian, Level Set Methods and Fast Marching Methods: Evolving Interfaces in Computational Geometry, Fluid Mechanics, Computer Vision, and Materials Science. Cambridge University Press, (1999) ISBN 0-521-64557-3.

[40] E. Olsson, G. Kreiss, A conservative level set method for two phase flow, J. Comput. Phys. 210 (1) (2005) 225-246.

[41] S. Osher, R. Fedkiw, Level Set Methods and Dynamic Implicit Surfaces, Springer, London.

[42] J.S. Eow, M. Ghadiri, A.O. Sharif, Experimental studies of deformation and break-up of aqueous drops in high electric fields, Colloids Surf. A: Physicochem.

Eng. Aspects. 225 (1-3) (2003) 193-210.

[43] G. Berg, L.E. Lundgaard, N. Abi-Chebel, Electrically stressed water drops in oil, Chem. Eng. Process. 49 (2010) 1229-1240.

[44] B. Li, Y. Fan, Z. Sun, Z. Wang, L. Zhu, Effects of high-frequency pulsed electrical field and operating parameters on dehydration of SAGD produced ultra-heavy oil, Powder Technol. 316(2017)338-344.

[45] C. Lesaint, W.R. Glomm, L.E. Lundgaard, J. Sjöblom, Dehydration efficiency of AC electrical fields on water-in-model-oil emulsions, Colloids Surf., A: Physicochem. Eng. Aspects. 352 (1-3) (2009), 63-69.

U(t)

8D

4D, earthed

(a)

2D D

$h_{max}/D=0.03$

(b)
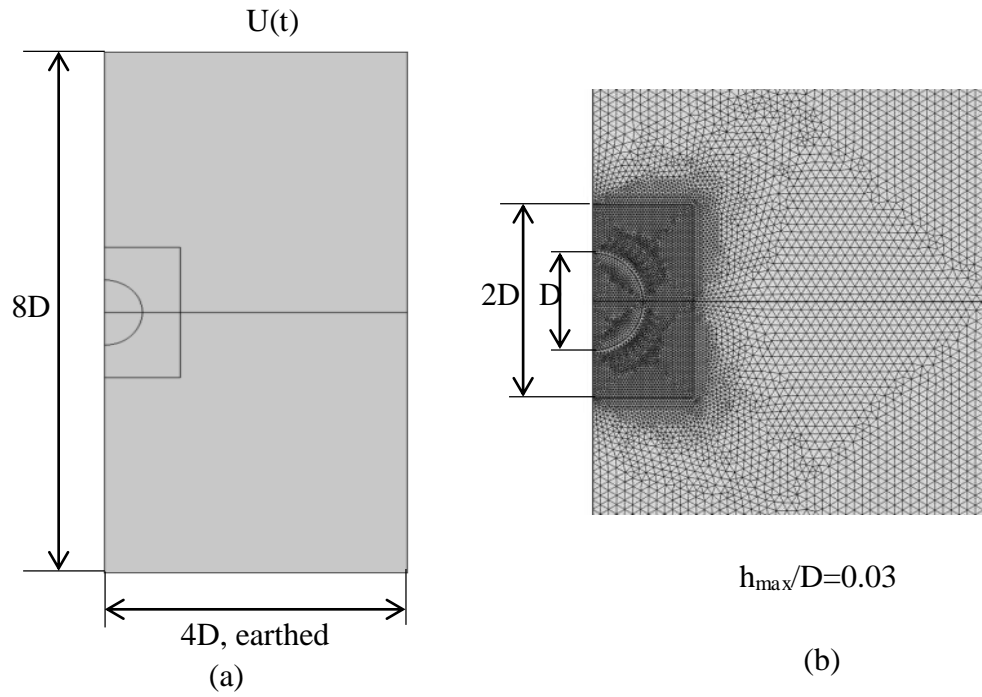
Fig. 1 (a) Schematic diagram of computational model. (b) Close-up of the mesh for $h_{max}/D=0.03$.
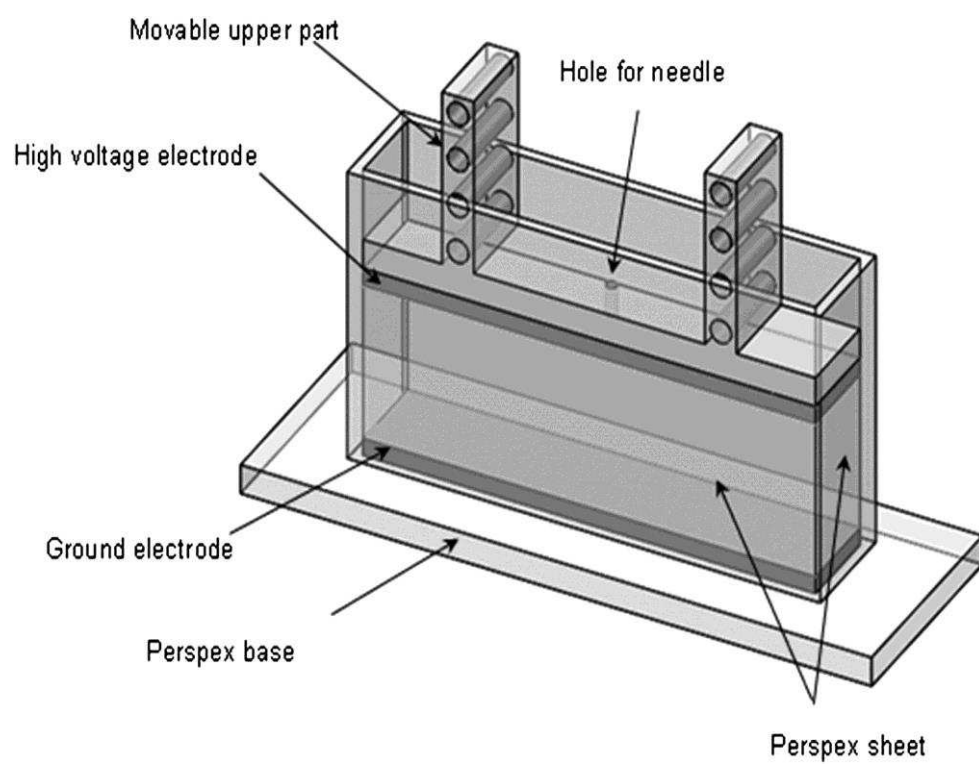
Fig. 2 Test cell [14, 42]

Electric field

(a)   (b)
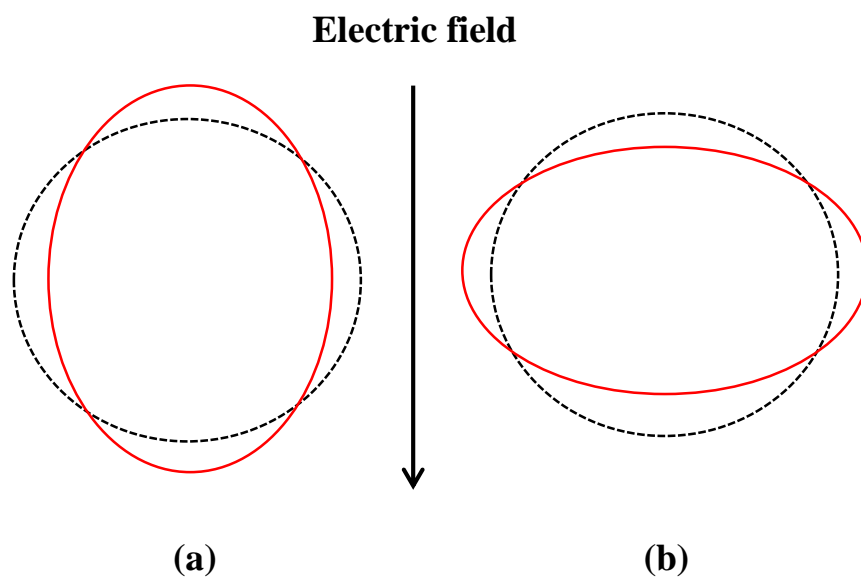
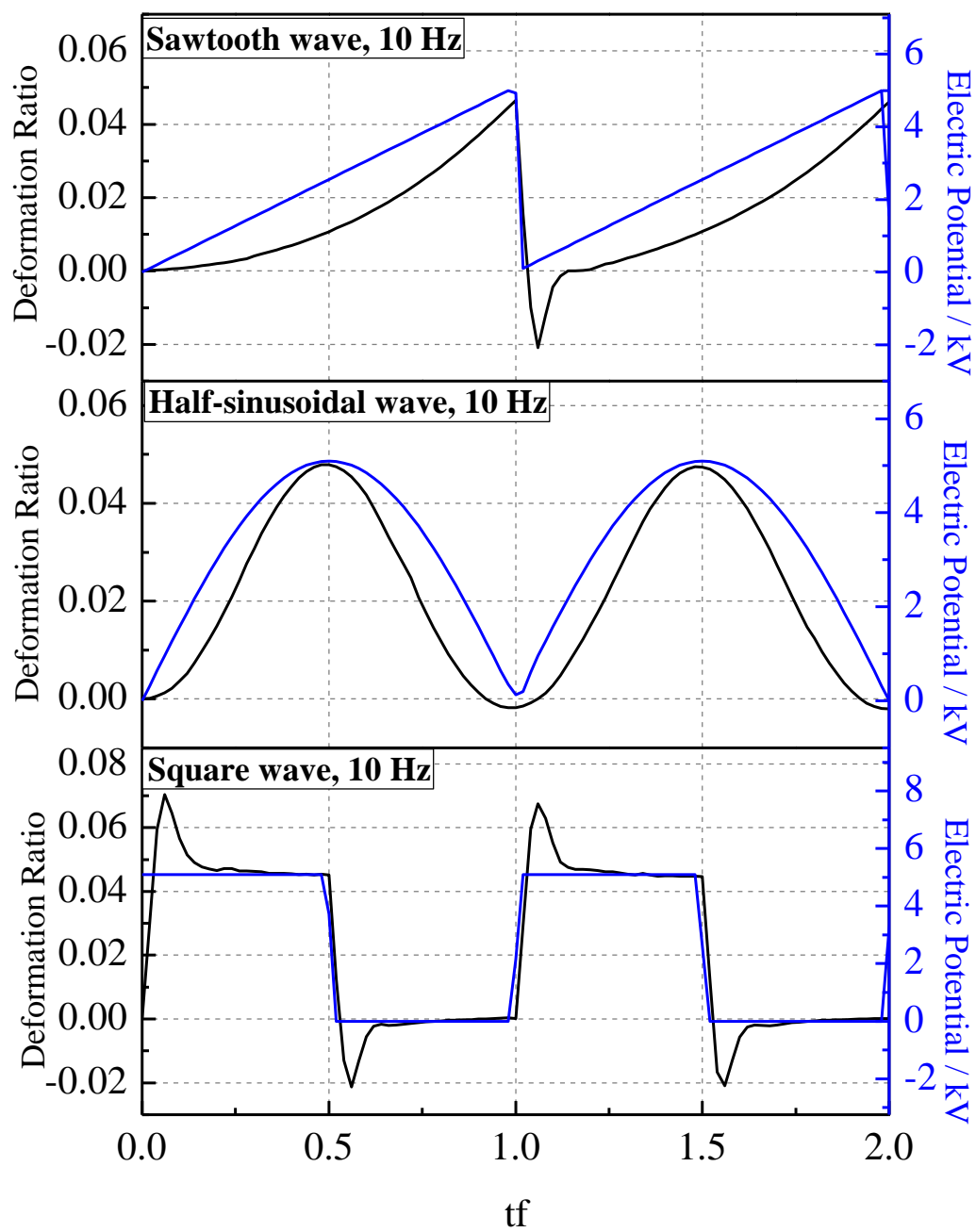**Fig.3 Droplet deformation patterns: (a) Dr>0, prolate shape; (b) Dr<0, oblate shape.**
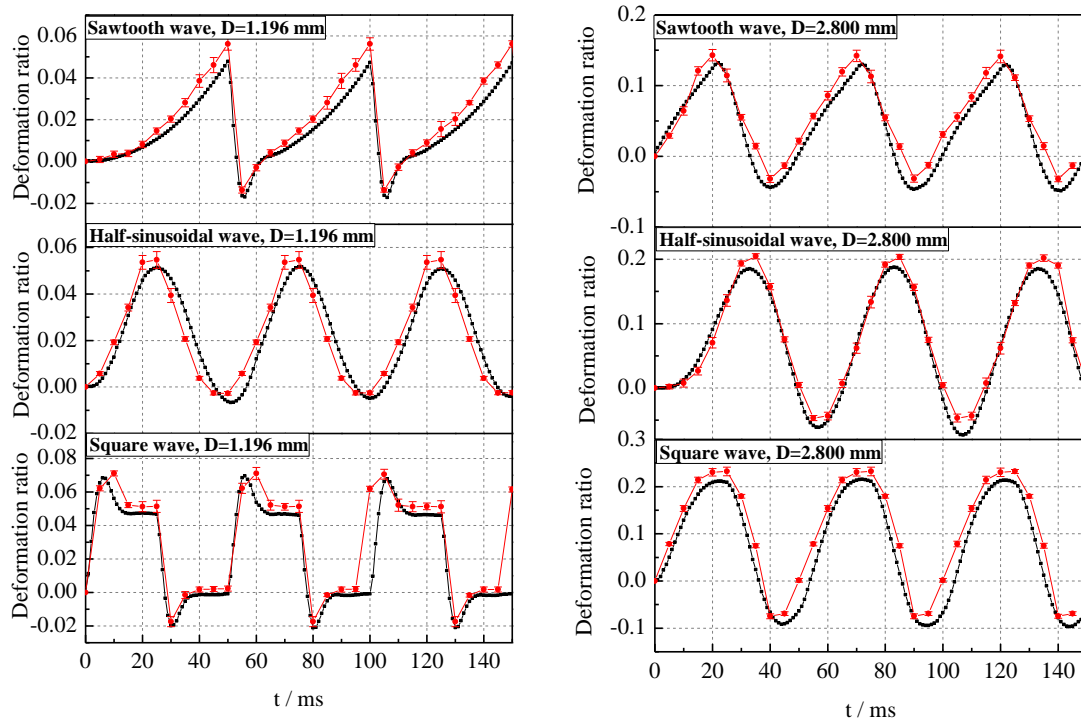
(a)
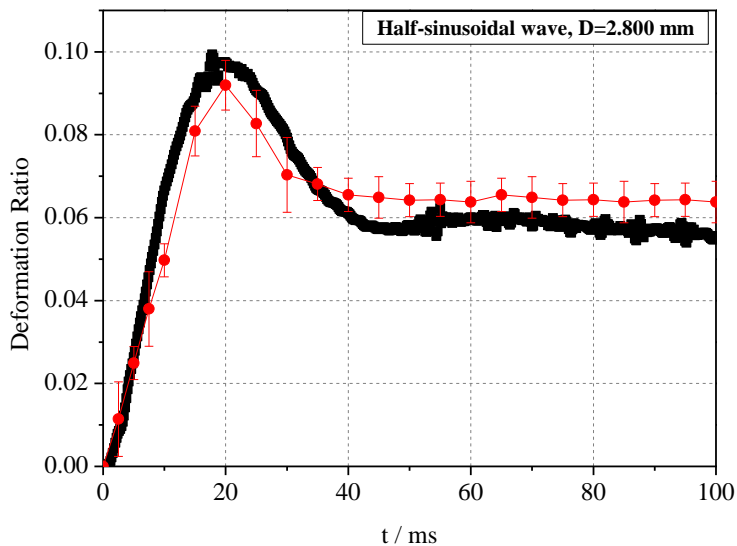
(b)

Fig. 4 Temporal profile of droplet deformation ratio obtained by simulation (▬■▬) and experimental (▬●▬) work. The parameters of numerical simulation work are identical to the experimental values (E=533 V mm^{-1},γ=0.025 N m^{-1}). (a): f=20 Hz; (b): Half-sinusoidal f=500 Hz.
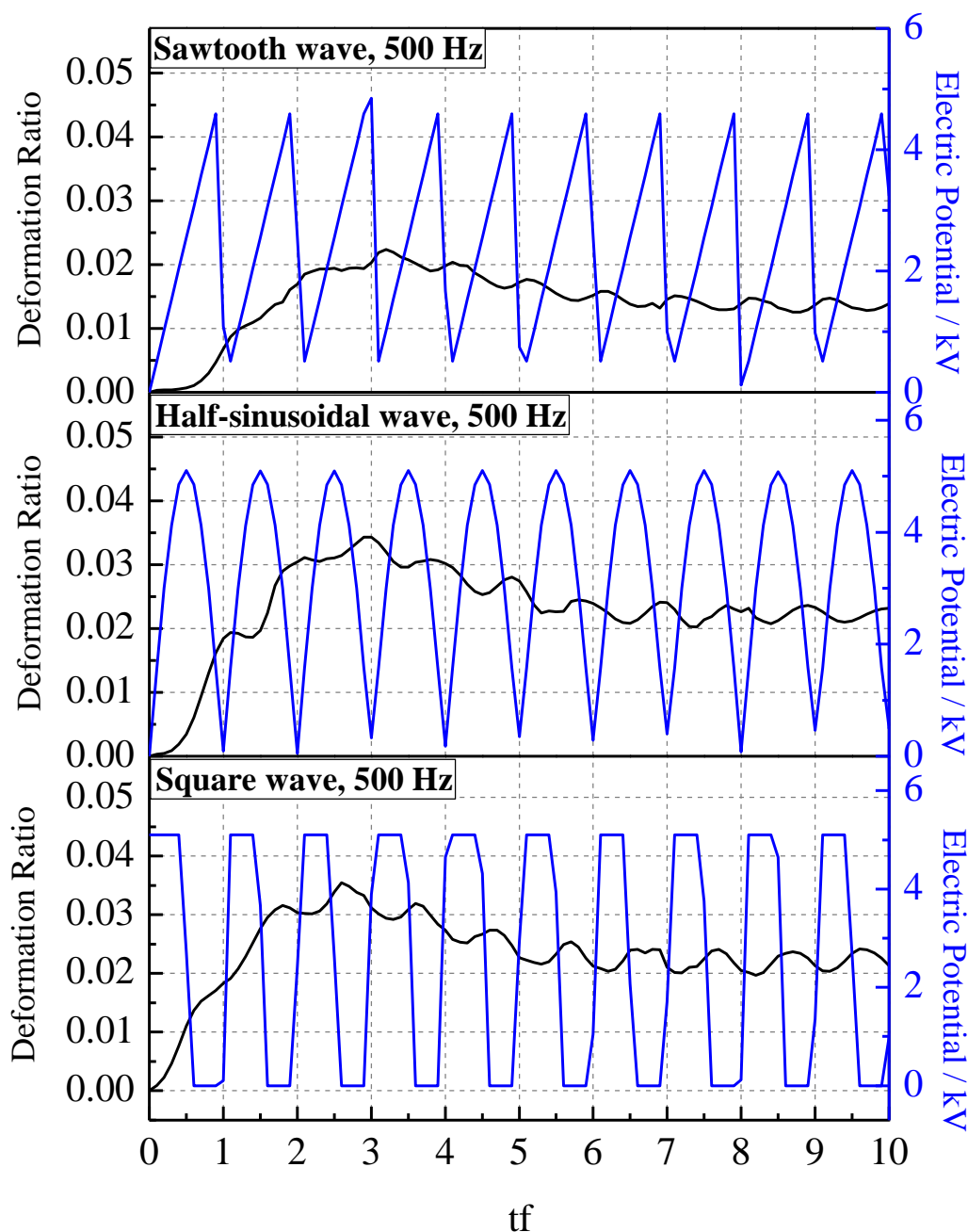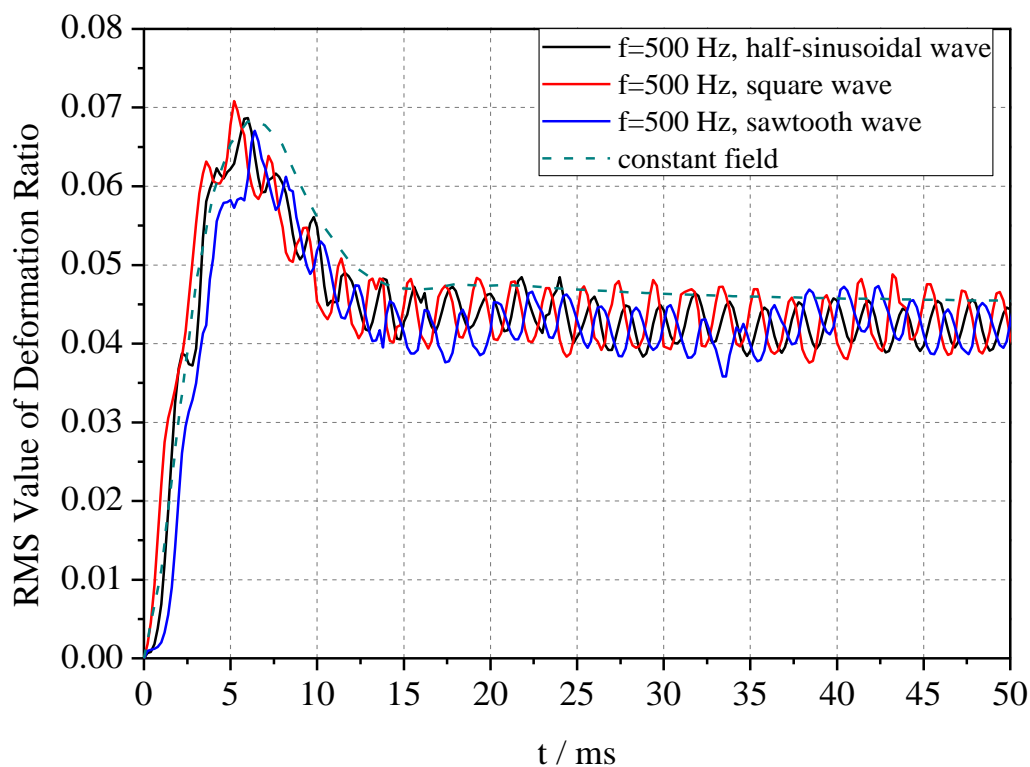
28

Fig. 5 (a)
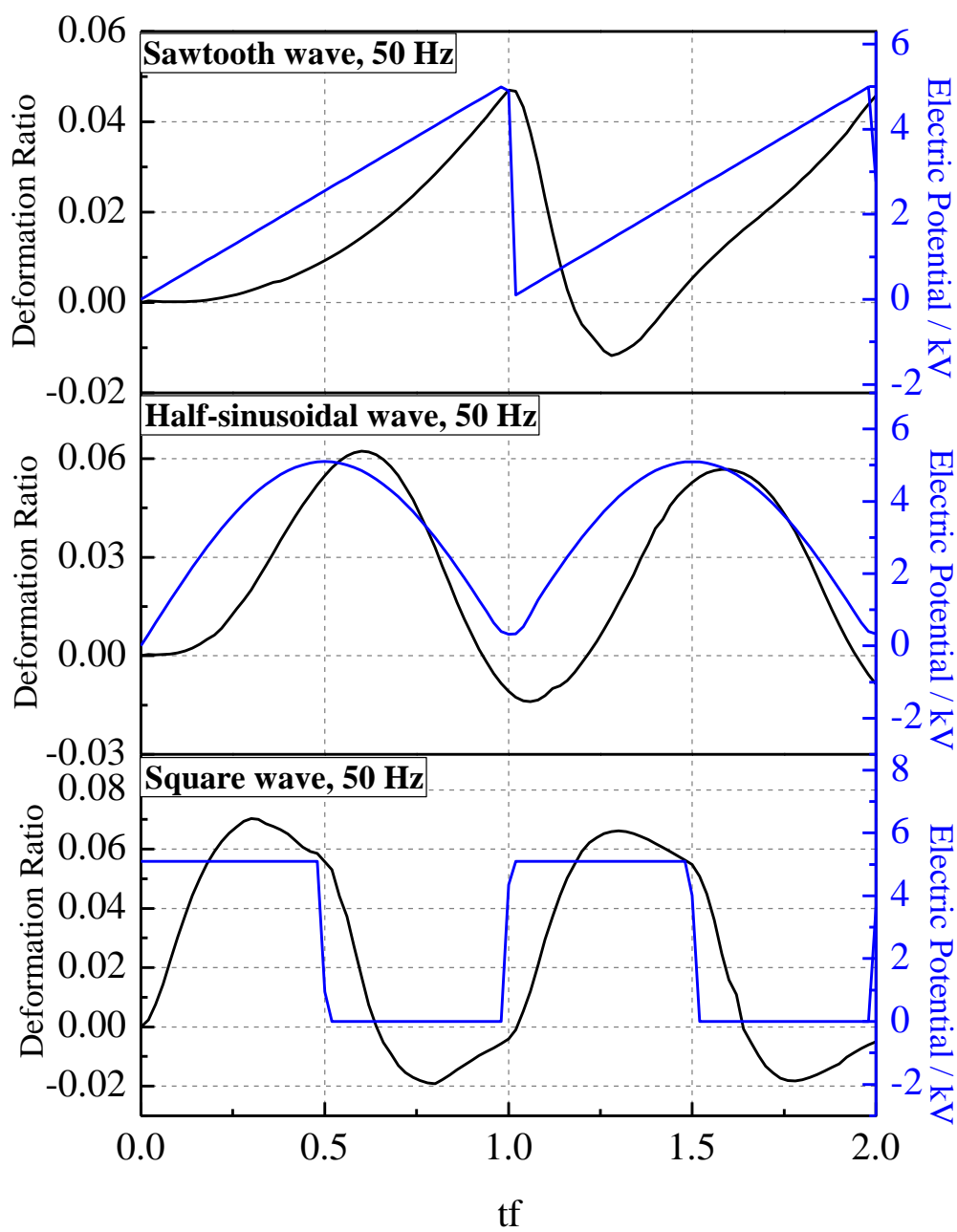
Fig. 5 (b)

Fig. 5 (c)

Fig. 5 Effect of electric field frequency on deformation under pulsatile fields: (a) 10 Hz; (b) 50 Hz; (c) 500 Hz. The calculation conditions are: E=533 V mm⁻¹, D=1.196 mm, γ=0.025 N m⁻¹ and fluids properties are given in Table 1. T=tf, where f is the frequency of the electric field.

Fig. 6 Droplet deformation process in constant, half-sinusoidal, square, and sawtooth waveform electric fields at 500 Hz. The RMS value of deformation ratio is plotted as function of time. The calculation conditions are: E=533 V mm^{-1}, D=1.196 mm, γ=0.025 N m^{-1} and fluids properties are given in Table 1.
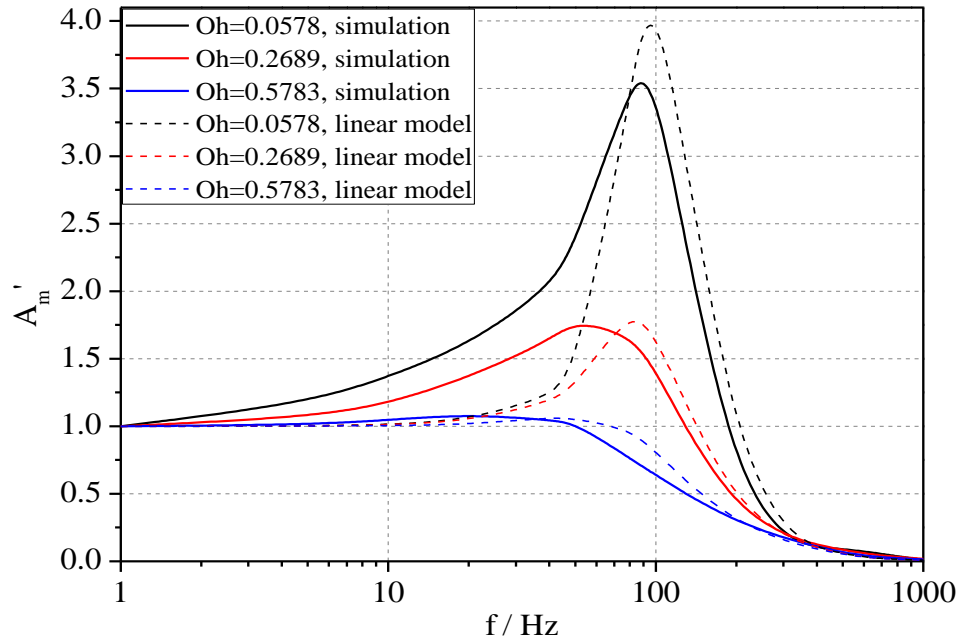
Fig. 7 Amplitude of the oscillatory response as a function of frequency and Ohnesorge Number. The calculation conditions are: E=533 V mm^{-1}, half-sinusodial wave.
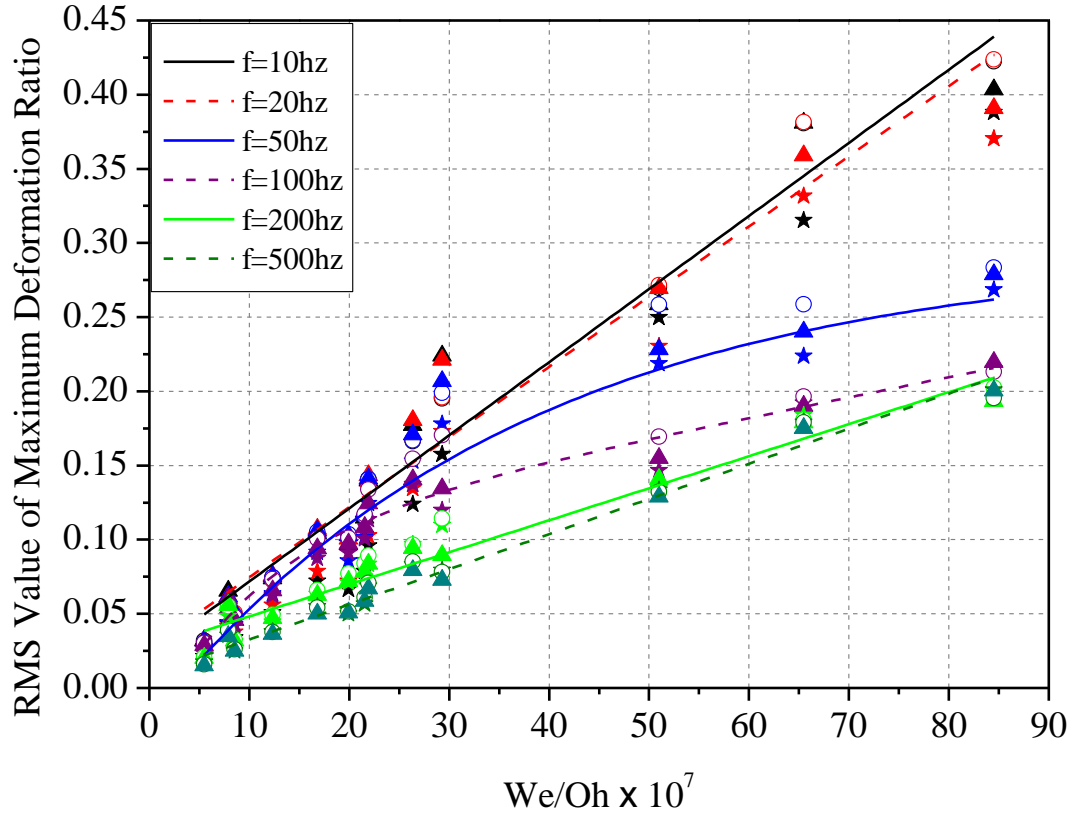
Fig. 8 RMS value of maximum deformation ratio as a function of the We/Oh number. The data points are calculated values for half-sinusodial (★), square (○) and sawtooth (▲) waves. The lines are fitted trend lines, using fluids properties given in Table 3.
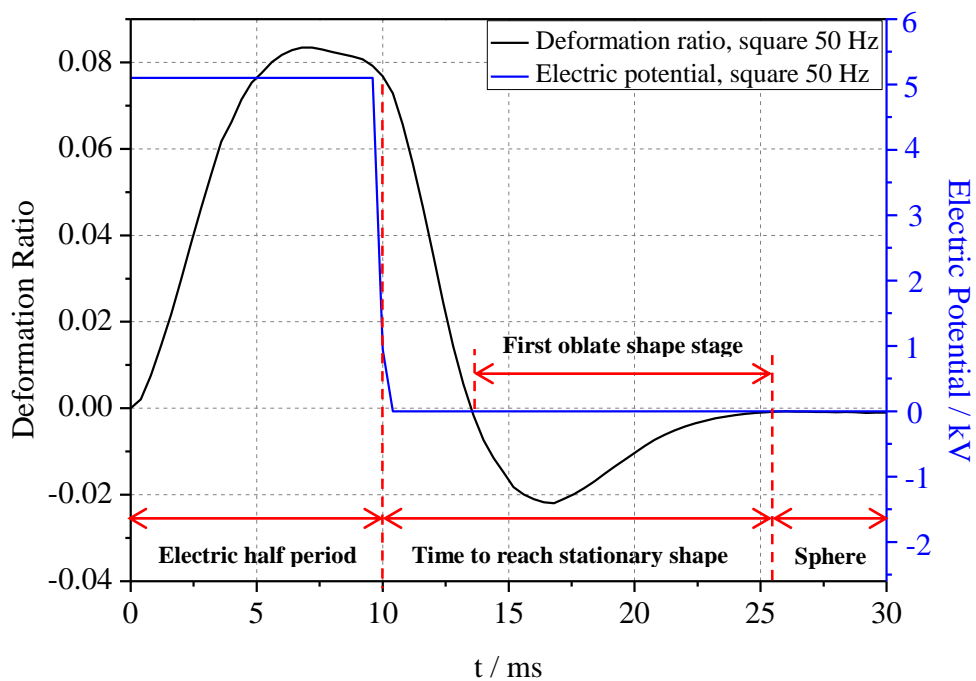
Fig. 9 The time to reach stationary shape (τ) obtained by applying a single step change under pulsatile fields. The calculation conditions are: square waveform; E=533 V mm^{-1}, D=1.196 mm, γ=0.020 N m^{-1} and fluids properties are given in Table 1.
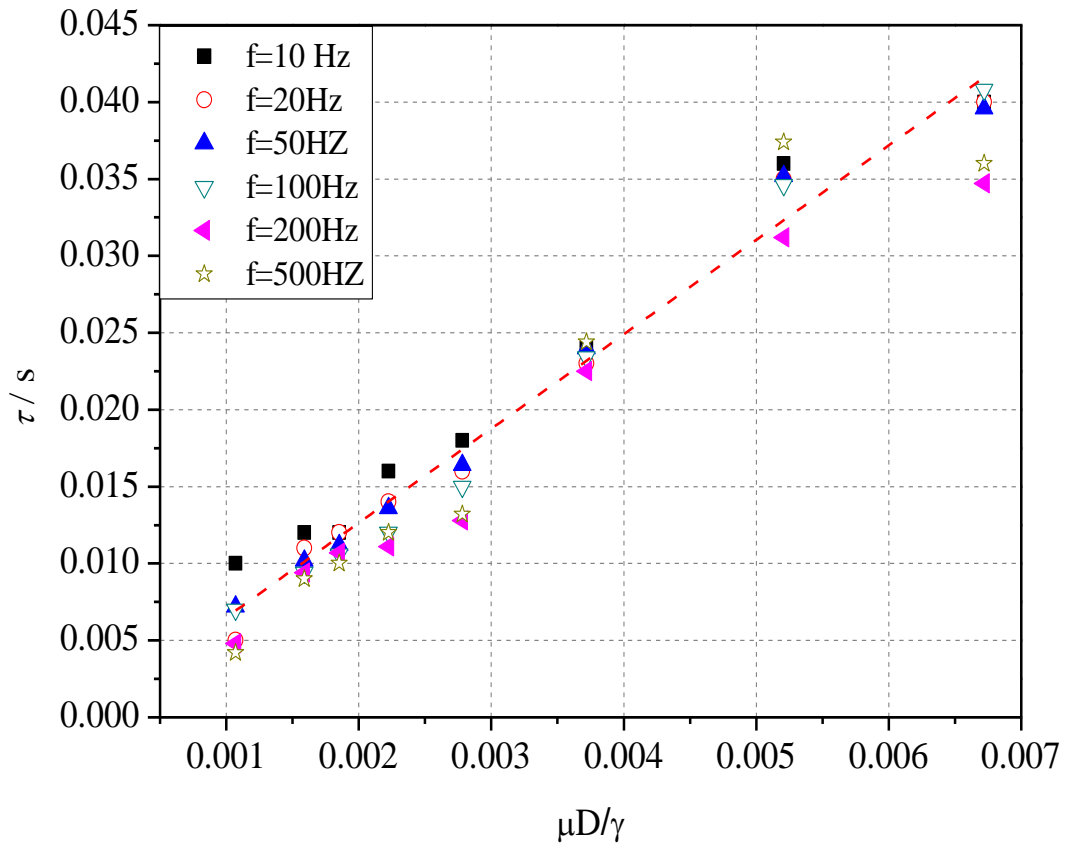
Fig. 10 Time to reach stationary shape (τ) as a function of dimensionless ratio (*μD/γ*) at different electric frequencies.

Table 1 Physical properties of the emulsion used in simulation [14]

Liquid	Conductivity (μs m^{-1}) ($\pm$5%)	Viscosity (mPa s)	Density (kg m^{-3})	Dielectric constant
Deionized water	5.49	1.0	1000	80.0
Sunflower oil	7.62$\times$10^{-5}	46.5	922	4.9

Table 2 Theoretical RMS values of the different electric field waveforms

Waveform	RMS
Half-sinusodial	$E_0 (\sqrt{2}/2)$
Square	$E_0 (\sqrt{2}/2)$
Sawtooth	$E_0 (\sqrt{3}/3)$
Constant	E_0

Table 3 Parameters used in We/Oh number calculation

We/Oh ($\times 10^7$)	Electric field strength (V/mm)	Droplet diameter (mm)	Surface tension (N/m)	Oil Viscosity (mPa s)
5.5	267	1.196	0.025	46.5
7.9	533	0.576	0.025	46.5
8.6	333	1.196	0.025	46.5
12.3	400	1.196	0.025	46.5
16.8	467	1.196	0.025	46.5
19.9	533	1.196	0.035	46.5
21.5	533	1.196	0.030	46.5
21.9	533	1.196	0.025	46.5
26.4	533	1.196	0.020	46.5
29.3	533	1.196	0.016	46.5
32.7	533	2.800	0.025	120.0
51.0	533	2.000	0.025	46.5
65.5	533	2.800	0.025	60.0
84.5	533	2.800	0.025	46.5

Table 4 Ratio of electric half period and τ (time to reach stationary shape)

We/Oh ($\times 10^7$)	10 Hz	20 Hz	50 Hz	100 Hz	200 Hz	500 Hz
5.5	3.13	1.79	0.74	0.42	0.23	0.08
7.9	5.00	5.00	1.39	0.71	0.52	0.24
19.9	4.17	2.27	0.98	0.53	0.27	0.11
21.5	4.17	2.08	0.89	0.47	0.23	0.10
26.4	2.78	1.56	0.61	0.33	0.20	0.08
51.0	2.08	1.09	0.42	0.21	0.11	0.04
65.5	1.25	0.63	0.25	0.12	0.07	0.03
84.5	1.39	0.71	0.28	0.14	0.08	0.03